

Effective Protection for Copper Corrosion by Two Thiazole Derivatives in Neutral Chloride Media: Experimental and Computational Study

Yujie Qiang¹, Shengtao Zhang^{1,*}, Shenyong Xu¹, Lei Guo², Nanxi Chen¹, Ime B. Obot³

¹ School of Chemistry and Chemical Engineering, Chongqing University, Chongqing 400044, P R China

² School of Materials and Chemical Engineering, Tongren University, Tongren 554300, P R China

³ Center of Research Excellence in Corrosion, King Fahd University of Petroleum and Minerals, Dhahran 31261, Saudi Arabia

*E-mail: stzhang_cqu@163.com

Received: 9 January 2016 / Accepted: 2 February 2016 / Published: 1 March 2016

Two corrosion inhibitors for copper in neutral NaCl solution, 2-aminobenzothiazole (ABT) and 2-amino-6-bromobenzothiazole (ABBT) were investigated by corrosion experiments and theoretical simulations. The results of weight loss and electrochemical experiments revealed that ABT and ABBT are efficient cathodic inhibitors with excellent inhibition efficiency (ABBT > ABT), which was further confirmed by field emission scanning electronic microscope (FESEM) observation. The adsorption of these molecules on copper surface was found to obey Langmuir adsorption isotherm. Moreover, the quantum chemical calculations and molecular dynamic (MD) simulation were used to investigate inhibition mechanism of studied inhibitors.

Keywords: Corrosion inhibitor, Adsorption, Copper, Electrochemical test, Quantum chemical calculation, Molecular dynamic simulation

1. INTRODUCTION

Ocean resources are applied more and more extensively to alleviate resource shortage problem in the earth. Meanwhile, copper is the most important metal used in marine engineering, including power stations, shipbuilding and seawater desalination, owing to their favorable thermal, electrical and mechanical properties [1]. However, corrosion is a serious global problem for some metallic material, causing approximate 3% loss of the global gross domestic product (GDP) [2]. Despite possessing excellent corrosive resistance, copper can be corroded seriously in marine environment due to the

existence of huge amounts of aggressive chloride ions. Thus, corrosion inhibition of copper in chloride media has attracted plenty of attention and has always being an important research topic [3-14].

In recent decades, numerous methods have been applied to prevent copper from corrosion in chloride containing environment. One of the most practical and cost-effective strategies is to employ organic compounds as corrosion inhibitors [15, 16]. Generally, these compounds usually contain conjugated double bonds, several heteroatoms (i.e. sulfur, nitrogen, oxygen) and/or polar functional groups [17-21]. Various organic compounds have been employed as inhibitors for corrosion of copper until now [16, 22-28], among which benzotriazole (BTA) and its derivatives are the most successful series due to the high performance and low costs. Many thiazole derivatives are explored as corrosion inhibitors for mild steel [29-32], and few of them have been employed for copper in acidic solution [33]. 2-mercaptobenzothiazole has also been proved as an effective inhibitor for copper corrosion [34, 35]. Furtherly, 2-aminobenzothiazole (ABT) and 2-amino-6-bromobenzothiazole (ABBT) were discovered for the first time by our group as more effective corrosion inhibitors for copper in 3% NaCl solution.

The purpose of the present study is to evaluate the inhibition mechanism of 2-aminobenzothiazole (ABT) and 2-amino-6-bromobenzothiazole (ABBT) for copper in chloride solution. Potentiodynamic polarization, electrochemical impedance spectroscopy (EIS), weight loss and FESEM techniques were used to evaluate the inhibitive performance of ABT and ABBT for copper corrosion in 3.0% NaCl solution at first. Both quantum chemical calculations and molecular dynamic simulation were further adopted to investigate the active sites and adsorption properties of these inhibitors on copper surface. Based on the results of experiments and theoretical calculations, an inhibitive mechanism is obtained to interpret the inhibition effects of studied organics for copper corrosion.

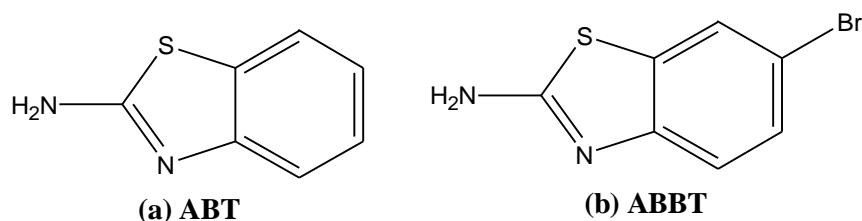


Figure 1. Molecular structure of (a) ABT and (b) ABBT

2. EXPERIMENTAL

2.1. Materials and sample preparation

Sodium chloride (NaCl, Aladdin, 99.9%), absolute ethanol (C₂H₅OH, Aladdin, 99.9%), ABT (Aladdin, 97%) and ABBT (Aladdin, 97%) as shown in Fig. 1 were used without any purification. For electrochemical experiments, the copper coupons (99.9%) with dimensions of 1.00 cm³ were embedded in epoxy resin leaving 1.00 cm² cross-sectional area exposed to the corrosive medium. Besides, the copper specimens for weight loss measurements were mechanically cut into 3.00 cm × 1.50 cm × 1.50 cm dimensions.

Prior to each experiment, the copper specimens were abraded consecutively with a series of emery papers (400, 800, 1600, 2000 grit). And then, they were washed ultrasonically with ultrapure water, degreased with acetone, and dried at room temperature before being immersed in testing solution. These corrosive media were prepared with adding ABT (0.1, 0.2, 0.3 and 0.4 mM) or ABBT (0.01, 0.05, 0.1 and 0.2 mM) into 3% NaCl solution. These concentrations of inhibitors are selected to obtain clear observation of inhibition ability. 10ml methanol was added to dissolve the compounds absolutely. Blank solution was also prepared with the same composition without corrosion inhibitor. All experiments were performed using calibrated thermostat at 298 ± 0.5 K.

2.2. Electrochemical measurements

Electrochemical experiments were conducted by CHI660B electrochemical workstation with conventional three-electrode system. A Bare copper electrode and a platinum plate were worked as the working electrode (WE) and the counter electrode (CE), respectively. Then a saturated calomel electrode (SCE) with a luggin capillary was used as the reference electrode (RE). All potential values reported were referred to SCE in present study.

Prior to each measurement, the WE was immersed in aggressive solution for 40 min at open circuit potential (OCP) to reach an almost steady state. Subsequently, EIS measurements were performed at the OCP in the frequency range from 100 kHz to 0.01 Hz using sinusoidal AC perturbation with amplitude of 5 mV. The EIS data were analyzed and fitted by Zsimpwin 3.10 software. At last, polarization experiments were performed in the potential range of ± 250 mV versus the OCP with a scan rate of 2 mV s^{-1} . The same experiment was carried out for 5 times to guarantee a favorable reproducibility.

2.3. Weight loss measurements

All of the weight loss experiments were carried out in 500 mL glass beakers placed in a thermostat water bath. Copper specimens in triplicate for each inhibitor concentration were weight and suspended in 3% NaCl solution for 10 days, respectively. Then the specimens were rinsed thoroughly in 0.1 mol/L HCl, water and acetone, subsequently dried before the determination of the loss in weight using analytical balance. The mean corrosion rates were finally calculated by the weight loss and immersion time of each specimen.

2.4. Surface analysis

In order to realize protection effects of the inhibitors on copper surface in corrosive media, the surface morphology of the copper specimens before and after immersed in 3% NaCl solution without and with 0.2 mM ABT and ABBT were investigated by field emission scanning electron microscope (FESEM, JEOL-JSM-7800F, Japan).

2.5. Calculation methods

Quantum chemical calculations were carried out by Gaussian 03W software. All molecules were fully optimized by density functional theory (DFT) using B3LYP functional with 6-311++G(d,p) basis set in aqueous phase. The corresponding quantum chemical parameters including the energy of the frontier molecule orbital (E_{HOMO} , E_{LUMO}), energy gap ($\Delta E = E_{\text{LUMO}} - E_{\text{HOMO}}$), and dipole moment (μ) are considered.

In addition, the forcite module in Material Studio 7.0 software was employed to explore the interaction between the Cu (111) surface and these inhibitors. The molecular dynamic (MD) simulation was performed in aqueous phase at 298 K, canonical ensemble (NVT), with a time step of 1.0 fs and simulation time of 500 ps.

3. RESULTS AND DISCUSSION

3.1. Potentiodynamic polarization curves

Representative Tafel polarization curves recorded on copper electrode in 3% NaCl solution in absence and presence of different concentrations of ABT and ABBT are shown in Fig. 2. With increase in the concentration of organic inhibitors, the polarization curves move directly to lower current densities, which is an indication that corrosion rate of copper has been decreased effectively. Furthermore, the shift to the lower current densities of the inhibited solution is more remarkable in the cathodic part of the polarization curves, and the corrosion potentials shift towards negative potentials compared with the blank. It may be inferred that the cathodic reaction of the corrosion process are suppressed primarily and thus protects copper from corrosion [36]. The results revealed that ABT and ABBT acted as modest cathodic inhibitors [37], and ABBT showed better inhibitive performance. Especially, with increasing the concentration of ABBT up to 0.2 mM, both of cathodic and anodic reactions are retarded evidently.

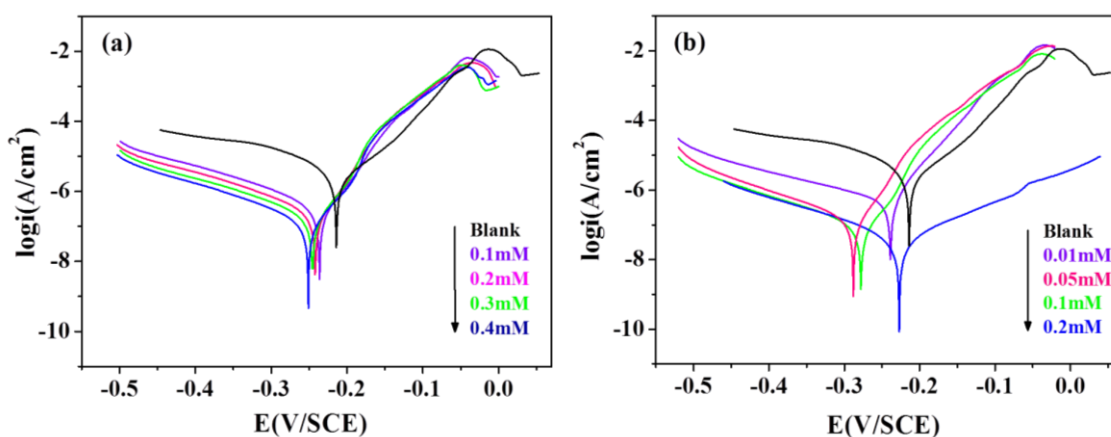


Figure 2. Potentiodynamic polarization curves for the copper electrode in 3% NaCl solution without and with different concentrations of (a) ABT and (b) ABBT at 298K

The cathodic and anodic i - E curves are extrapolated up to their intersection points where corrosion potential (E_{corr}) and corrosion current density (i_{corr}) are obtained [28, 38]. The key electrochemical parameters, including E_{corr} , i_{corr} , anodic and cathodic Tafel slope (β_a , β_c), and inhibition efficiency (η) are shown in Table 1. The values of η are calculated using the following equation:

$$\eta = \frac{i_{\text{corr},0} - i_{\text{corr}}}{i_{\text{corr},0}} \times 100 \quad (1)$$

where $i_{\text{corr},0}$ and i_{corr} indicate uninhibited and inhibited current densities of copper specimen, respectively. Table 1 reveals that corrosion current densities (i_{corr}) decrease obviously when organic inhibitors are present. These values of i_{corr} continue to reduce and the inhibition efficiencies that calculated from i_{corr} increase with incremental concentration of these inhibitors. The values of η for ABT and ABBT at each concentration are extremely high, and the maximum values of the efficiencies are 96.3% with ABT at 0.4 mM and 98.4% with ABBT at 0.2 mM. These results indicate that effectively protective film of inhibitor molecules are formed on the copper surface [27]. This film acts as a barrier to the diffusion of oxygen molecules from the solution to the copper surface, and thus blocks the active sites on the copper surface to protect corrosion of copper [22, 39].

Table 1. Potentiodynamic polarization parameters for copper in 3% NaCl solution without and with different concentrations of ABT or ABBT at 298K

C (mM)	E_{corr} (mV/SCE)	i_{corr} ($\mu\text{A cm}^{-2}$)	β_c (mV s^{-1})	β_a (mV s^{-1})	η (%)
Blank	-214	2.750	-94	59	—
ABT					
0.1	-176	0.295	-141	41	89.3
0.2	-182	0.208	-134	38	92.9
0.3	-186	0.152	-139	36	94.8
0.4	-191	0.108	-136	38	96.3
ABBT					
0.01	-179	0.580	-195	41	78.9
0.05	-228	0.129	-141	38	95.3
0.1	-218	0.077	-149	36	97.2
0.2	-167	0.044	-122	114	98.4

3.2. Electrochemical impedance spectroscopy

In order to get insight into the corrosion mechanism and verify the results of polarization experiments, electrochemical impedance spectroscopic investigations of copper in 3% NaCl solution without and with different concentrations of inhibitors were carried out. Corresponding Nyquist and Bode plots are given in Fig. 3.

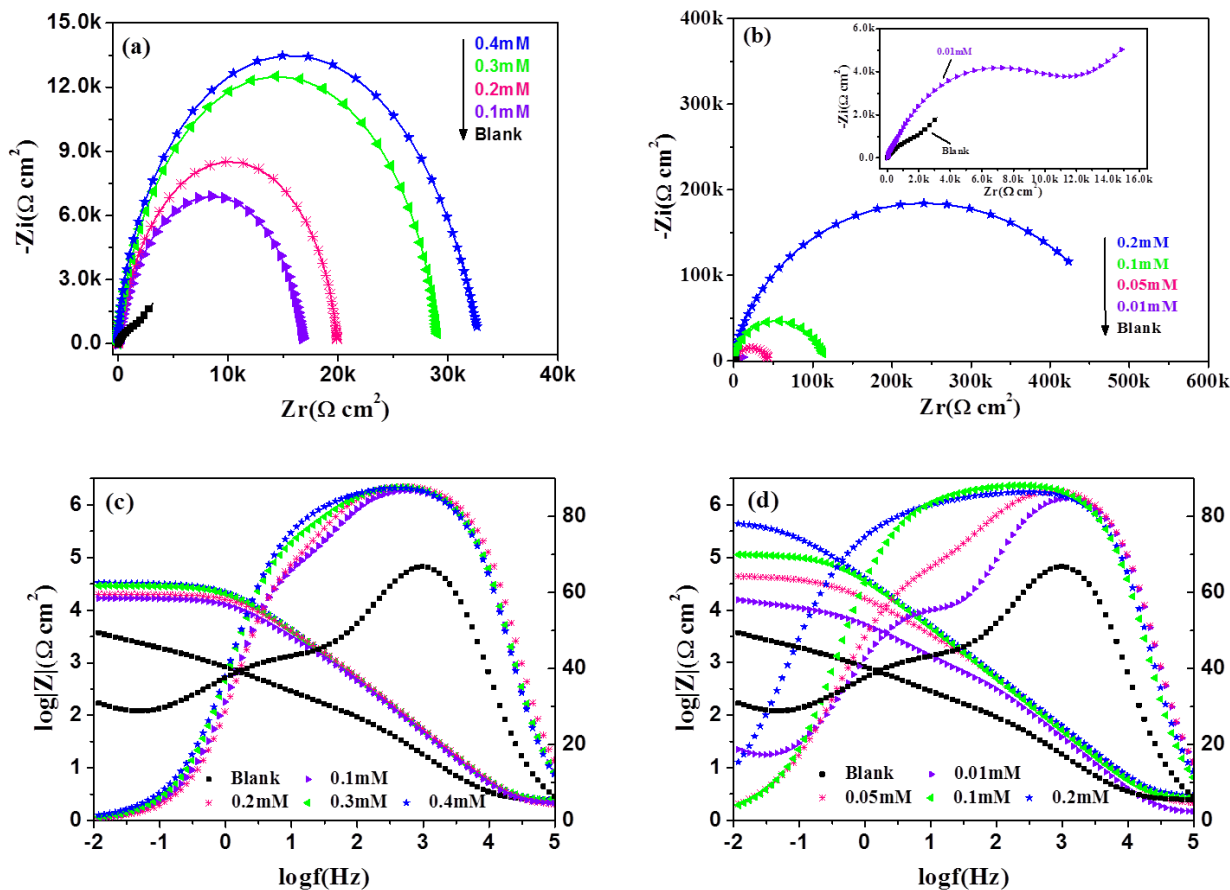


Figure 3. Nyquist and Bode plots for copper in 3% NaCl solution without and with different concentration of ABT (a,c) and ABBT (b,d) at 298 K.

As shown in Fig. 3a and Fig. 3b, the Nyquist plots of the blank solution of both inhibitors and 0.01mM ABBT show an imperfect semicircle in the high frequency region followed by a straight line at low frequency range.

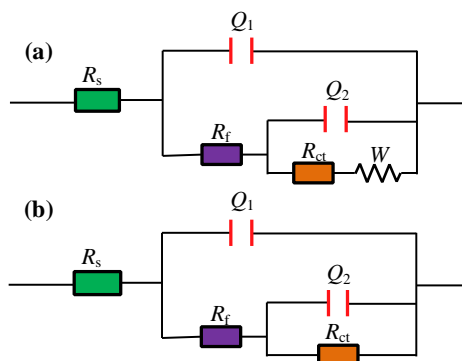


Figure 4. Equivalent circuits used to fit the EIS data (a) with and (b) without Warburg impedance

Generally, the high frequency semicircle is relevant to the resistance of charge transfer (R_{ct}) and double layer capacitance (C_{dl}). The low frequency impedance is deemed as Warburg impedance

(W), which can be interpreted by the transportation of soluble cuprous chloride complexes from copper surface to the bulk solution or the diffusion of dissolved oxygen to the surface of copper [40]. It can be seen that Warburg impedance disappears with increasing concentration of these inhibitors. Only some large convex arcs are noticed in the Nyquist plots, demonstrating that corrosion process is controlled by the charge transfer step in such conditions. Besides, each diameter of the semicircle increases obviously with increasing concentration of ABT and ABBT.

The increase of $\log|Z|$ at low frequencies in Bode plots (Fig. 3c and Fig. 3d) shows the higher protection performance with incremental concentration of these inhibitors. In addition, large values of the phase angle are observed and then continue to become higher with increasing concentration of inhibitors, indicating that superior inhibition behavior is obtained due to more and more inhibitor molecules adsorbed on copper surface at higher concentration.

Generally, the impedance data could be properly fitted using the equivalent circuits shown in Fig. 4. The corresponding electrochemical parameters obtained from the equivalent circuits are listed in Table 2. Here, R_s is the solution resistance, R_f reflects the resistance of protective film formed on copper surface, W represents the Warburg impedance and R_{ct} represents the charge transfer resistance. Q_f and Q_{dl} are constant phase angle elements (CPE), denoting a film capacitance (C_f) and double-layer capacitance (C_{dl}), respectively. These circuits in this case could be expressed as follows [36],

$$Z_{(\text{with } W)} = R_s + \frac{1}{j\omega CPE_f + \frac{1}{R_f} + \frac{1}{j\omega CPE_{dl} + \frac{1}{R_{ct} + W}}} \quad (2)$$

$$Z_{(\text{without } W)} = R_s + \frac{1}{j\omega CPE_f + \frac{1}{R_f} + \frac{1}{j\omega CPE_{dl} + \frac{1}{R_{ct}}}} \quad (3)$$

The impedance of CPE is defined as follows [41],

$$Z_{CPE} = \frac{w^{-n}}{Y \left(\frac{\cos n\pi}{2} + j \frac{\sin n\pi}{2} \right)^n} \quad (4)$$

where Y is the modulus of the CPE, w is the angular frequency, j is the imaginary number ($j^2 = -1$), n is the deviation parameter, denoting the meaning of a phase shift. When $n = 0$, the CPE indicates a pure resistor, for $n = +1$, a pure capacitor, and for $n = -1$, an inductor.

In addition, the values of η of these inhibitors for the copper electrode in 3% NaCl solution are calculated from the polarization resistance R_p ($R_p = R_{ct} + R_f$) as follows,

$$\eta = \frac{R_p - R_{p,0}}{R_p} \times 100 \quad (5)$$

where R_p and $R_{p,0}$ are the sum of charge transfer resistance and film resistance for copper in 3% NaCl media without and with inhibitors, respectively.

Obviously, in Table 2, the values of both R_{ct} and R_f increase with the addition of ABT or ABBT, and this effect are enhanced by increasing their concentration, demonstrating that a high-efficiency protective film are formed by the adsorption effect of these inhibitors on copper surface.

Furthermore, the values of C_f and C_{dl} , which can be expressed as equations (6) and (7) below in the present study [42, 43], exhibits a decreasing trend with increasing concentration of inhibitors.

$$C_{dl} = \frac{\epsilon^0 \epsilon}{d} S \quad (6)$$

$$C_f = \frac{F^2 S}{4RT} \quad (7)$$

Table 2. Impedance parameters recorded for copper electrode in 3% NaCl solution in the absence and presence of ABT and ABBT at 298K

C (mM)	R_s ($\Omega \text{ cm}^2$)	R_f ($\text{k}\Omega \text{ cm}^2$)	R_{ct} ($\text{k}\Omega \text{ cm}^2$)	C_f (μF cm^{-2})	n_1	C_{dl} (μF cm^{-2})	n_2	W	η (%)
Blank	2.40	0.10	2.5	18.62	0.92	347	0.56	0.00128	—
ABT									
0.1	2.12	2.95	13.9	3.43	1	7.53	0.8	—	84.6
0.2	1.97	5.41	14.5	2.94	0.99	5.42	0.83	—	86.9
0.3	2.34	5.54	23.6	3.09	0.97	4.19	0.78	—	91.1
0.4	2.40	6.12	42.3	3.20	1	4.28	0.64	—	94.6
ABBT									
0.01	1.42	0.66	11.2	4.25	1	3.67	0.71	0.0006	78.1
0.05	2.11	2.23	43.0	2.82	1	11.1	0.67	—	94.3
0.1	2.63	4.59	113.4	3.10	0.98	2.41	0.58	—	97.8
0.2	2.88	4.63	512.2	2.68	0.99	2.54	0.65	—	99.5

where S is the surface area of copper electrode exposed to corrosive medium, d is the thickness of electric double-layer, F is the Faraday's constant. ϵ^0 and ϵ show the permittivity of the air and the local dielectric constant, respectively. Thus, the decrease of C_f can be interpreted with the adsorption effect of these organic molecules, which reduces the exposed electrode surface area at higher inhibitor concentration and thereby retards copper corrosion efficiently. Furthermore, water molecules on the electrode surface are replaced gradually by inhibitor molecules at the metal/solution interface, leading to thicker electric double-layer, lower local dielectric constant, and smaller exposed electrode surface area mentioned above. All these factors result in reduce of C_{dl} [39].

Consequently, inhibition efficiencies increase with the inhibitor concentration and reach 94.6% for ABT at 0.4 mM, 99.5% for ABBT at 0.2 mM, respectively. It indicates that these compounds act as effective corrosion inhibitor for copper in 3% NaCl medium. These results are in good agreement with those obtained from polarization measurements and provide further confirmation about corrosion process.

3.3. Weight loss measurements

The effect of ABT and ABBT addition at different concentrations for copper corrosion in 3% NaCl solution was investigated by weight loss measurement at 298 K after 10 days immersion. The

corrosion rate (W , $\text{mg m}^{-2} \text{h}^{-1}$) and inhibition efficiency (η) at various concentrations of these compounds are listed in Table 3. η can be calculated by,

$$\eta = \frac{W^0 - W}{W^0} \times 100 \quad (8)$$

where W^0 and W are the corrosion rates of copper in 3% NaCl solution without and with the inhibitors, respectively. The corrosion rates decrease distinctly, meanwhile the inhibition efficiencies increases obviously with increasing concentration of these inhibitors as seen from Table 3. Both of these inhibitors retard the copper corrosion effectively in 3% NaCl solution at all concentrations, which indicates good inhibitive capacity of these compounds. The maximum efficiency reaches 92.7% with ABT at 0.4 mM and 94.9% with ABBT at 0.2 mM. Furtherly, it is discovered that the inhibition efficiencies obtained from weight loss measurements are in accordance with those from the electrochemical experiments.

Table 3. Corrosion parameters obtained from weight loss measurements of copper specimens in 3% NaCl solution containing different concentrations of ABT and ABBT at 298K

C (mM)	W ($\text{mg m}^{-2} \text{h}^{-1}$)	η (%)
Blank	8.06	—
ABT		
0.1	1.36	83.1
0.2	1.18	85.4
0.3	0.87	89.2
0.4	0.59	92.7
ABBT		
0.01	1.98	75.4
0.05	0.73	91.0
0.1	0.53	93.4
0.2	0.41	94.9

3.4. Morphological analysis

FESEM is widely used to study the effects of corrosion inhibition through morphological characteristics of metal surface [14, 25, 44-47]. Fig. 5 shows the high-definition photographs of the copper coupons before and after the immersion in 3% NaCl solution for 7 days in absence and presence of 0.2 mM inhibitors. The copper specimen in 3% NaCl solution without inhibitors (Fig. 5b) is strongly corroded by the aggressive solution, and the surface of this specimen becomes rough, scratched and porous obviously. In contrast, in the presence of 0.2 mM ABT (Fig. 5c) and ABBT (Fig. 5d), the surface of the specimens is well protected and the micrographs are nearly the same as the freshly polished copper (Fig. 5a). Therefore, it can be concluded that both of these compounds are good inhibitors for copper corrosion even at a low concentration. These observations confirm that, protective layers on the copper surface are formed by these two kinds of organic molecules, which prevents the attack of corrosive media and thereby reducing the corrosion rate effectively.

Furthermore, the specimen surface with ABBT is smoother slightly than counterpart with ABT, which also support the results obtained from electrochemical and weight loss experiments.

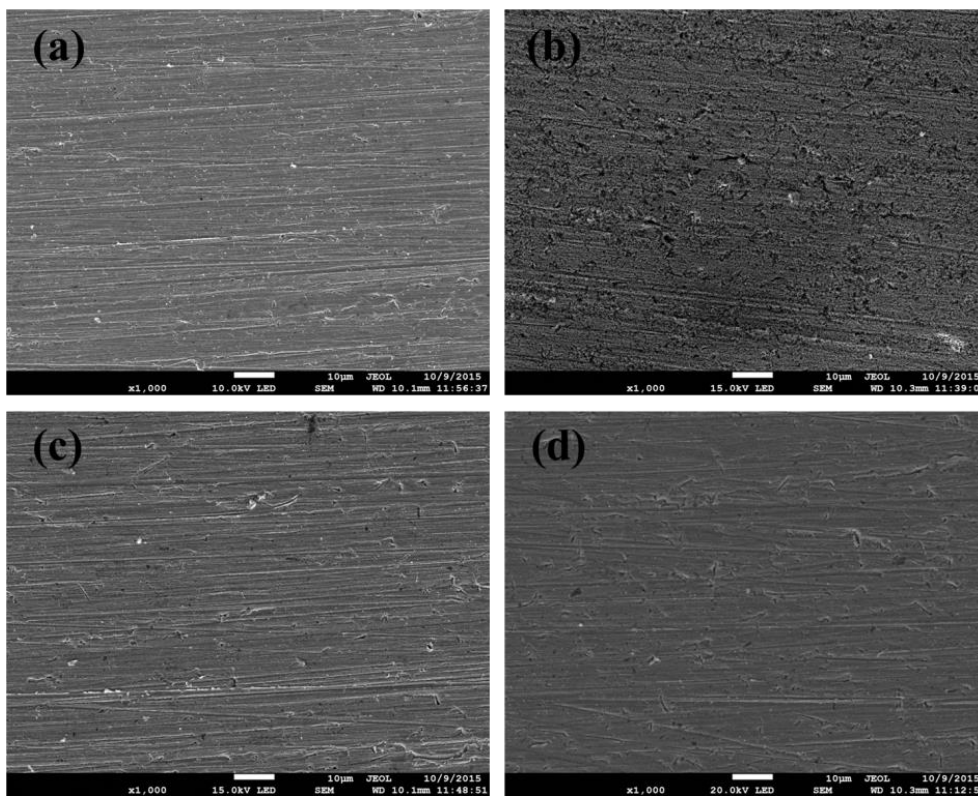


Figure 5. FESEM micrographs of (a) freshly polished copper specimen and the specimens immersed in 3% NaCl solution for 7 days (b) without inhibitor and (c) with 0.2 mM ABT and (d) 0.2 mM ABBT

3.5. Adsorption isotherm studies

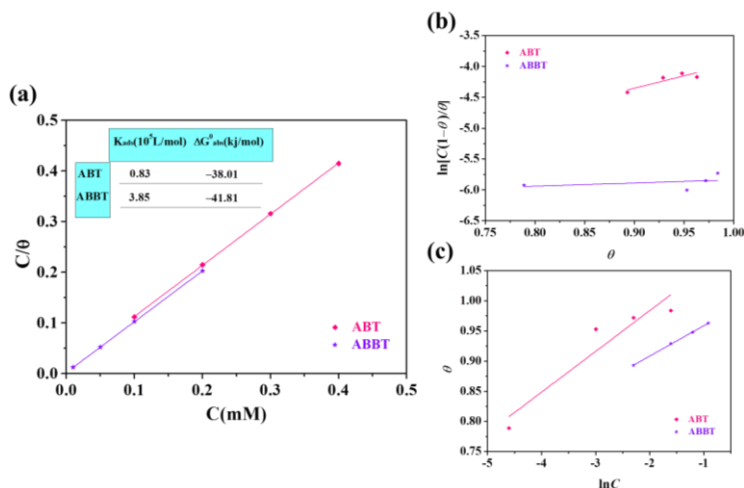


Figure 6. (a) Langmuir adsorption isotherm and corresponding thermodynamic parameters of ABT and ABBT on the copper surface in 3% NaCl solution at 298K, (b) Frumkin isotherm plot, (c) Temkin isotherm plot, respectively.

As known, adsorption isotherm is extensively employed to investigate the adsorption mechanism of corrosion inhibitor on metal/solution interface. In present study, several classical adsorption isotherms including Langmuir, Frumkin, and Temkin isotherms [48-50] as shown in Fig. 6 are used to fit the results obtained from potentiodynamic polarization measurements of the organic compounds.

$$\frac{\theta}{1-\theta} = K_{\text{ads}} C \quad (\text{Langmuir isotherm}) \quad (9)$$

$$\left(\frac{\theta}{1-\theta}\right) \exp(2a\theta) = K_{\text{ads}} C \quad (\text{Frumkin isotherm}) \quad (10)$$

$$\exp(-2a\theta) = K_{\text{ads}} C \quad (\text{Temkin isotherm}) \quad (11)$$

where θ , the degree of the coverage, is defined as η (%), C is the concentration of the compounds, K_{ads} is the equilibrium constant of adsorption process of corrosion inhibitors and a is the molecular interaction parameter.

As seen in Fig. 6, Langmuir isotherm was found to be the most suitable mode to fit experimental results, with all linear regression coefficients (R^2) very close to 1, whereas Frumkin isotherm (ABT: 0.676, ABBT: 0.461), Temkin isotherm (ABT: 0.853, ABBT: 0.981), respectively. It suggests that adsorption process of ABT and ABBT on copper surface in 3% NaCl solution obeys Langmuir isotherm. The relationship between C and C/θ complies straight lines with intercept of $1/K$. The standard free energy of adsorption (ΔG_{ads}^0) can be calculated as follows [51-53],

$$K_{\text{ads}} = \frac{1}{55.5} \exp\left(\frac{-\Delta G_{\text{ads}}^0}{RT}\right) \quad (12)$$

Here, T is the absolute temperature (K), 55.5 is the molar concentration of water in the solution (mol/L) and R is the molar gas constant ($8.314 \text{ J mol}^{-1} \text{ K}^{-1}$).

Thermodynamic parameters obtained are also shown in Fig. 6. Generally, a high value of K_{ads} and low value of ΔG_{ads}^0 demonstrate that the inhibitor could be easily and strongly adsorbed on the metal surface, indicating a superior inhibition behavior [54]. It can be seen that the values of K_{ads} and ΔG_{ads}^0 follow the order: $K_{\text{ads}}(\text{ABBT}) > K_{\text{ads}}(\text{ABT})$, $\Delta G_{\text{ads}}^0(\text{ABBT}) < \Delta G_{\text{ads}}^0(\text{ABT})$, indicating that ABBT exhibits a better inhibitive performance than ABT, which is agreement with experimental results mentioned above.

Besides, the negative values of ΔG_{ads}^0 indicate that the adsorption of these inhibitors on copper surface is a spontaneous process. As is well known that the value of ΔG_{ads}^0 around or lower than -40 kJ/mol is consistent with chemisorption owing to the covalent bond formed by charge transfer or sharing from the inhibitor molecules to the surface of copper. If the ΔG_{ads}^0 value is around or higher than -20 kJ/mol, it can be regarded as physisorption. The corresponding corrosion inhibition acts by electrostatic interaction between the charged metal and the charged organic molecules [55]. Thus corrosion inhibition process of ABT on copper surface is mixed adsorption between physisorption and chemisorption, while stronger chemisorption could take place for ABBT in same condition. These results further confirm that ABBT is a more effectively corrosion inhibitor of copper in 3% NaCl medium than ABT.

3.6. Quantum Chemical Calculations

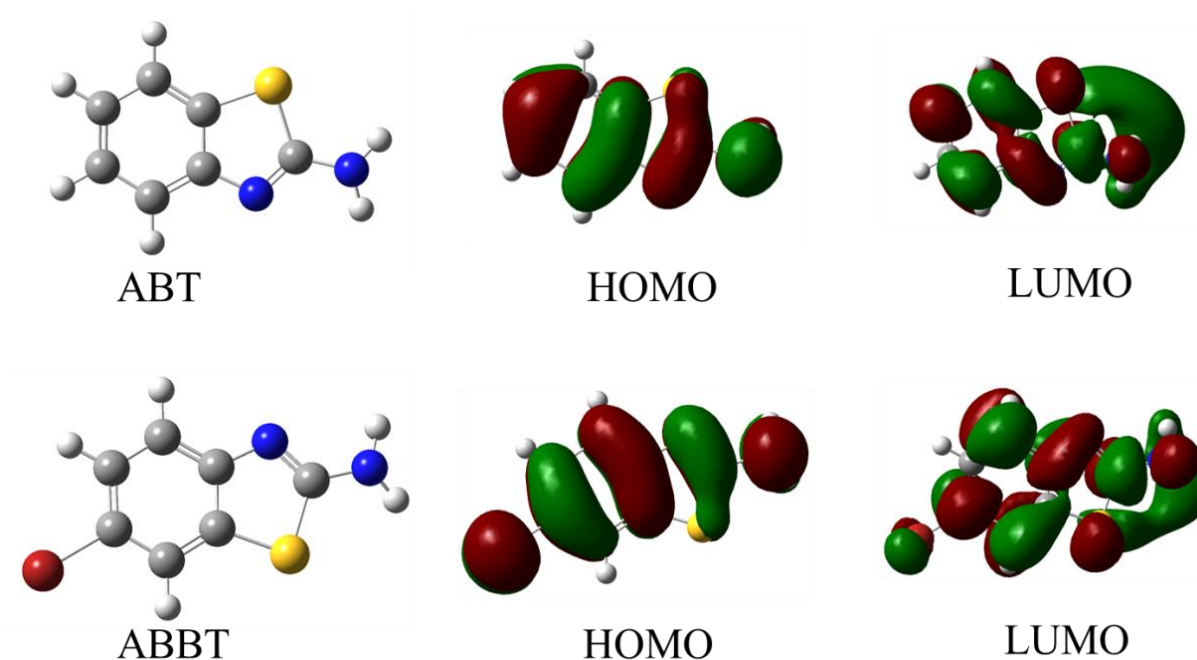


Figure 7. Optimized molecular structures and frontier molecular orbital of ABT and ABBT

Quantum chemical calculations are widely used in studying the correlation between molecular structure and inhibition mechanism in corrosion field[56]. Thus in the present work, density functional theory (DFT) were employed to investigate the inhibition effect of both ABT and ABBT on copper surface. The fully optimized geometry structure, density distribution of the highest occupied molecular orbital (HOMO) and the lowest unoccupied molecular orbital (LUMO), contour and total electron density surface of electrostatic potential (ESP) of these inhibitor molecules are given in Fig. 7 and Fig. 8. Besides, the computed quantum chemical parameters such as the energy of the frontier molecule orbital (E_{HOMO} , E_{LUMO}), energy gap ($\Delta E = E_{\text{LUMO}} - E_{\text{HOMO}}$), and dipole moment (μ) are listed in Table 4. As shown in Fig. 7, both of these organic molecules are plane conjugated structure, which imply that flat mode with the largest contact area may be obtained if the inhibitors absorbed on the surface of copper. In addition, the HOMO and LUMO for both of these inhibitors distribute almost whole region of the thiazole and aromatic rings. The planar structure could thus to be absorbed on copper surface with several feasible active centres for the interaction [27]. Moreover, as known that negative (red) regions of the ESP map in Fig. 8 are associated with nucleophilic reactivity, meanwhile the positive (blue) regions with electrophilic reactivity. Generally, metal acting as an electrophilic agent is accessible to attract negatively charged sites of inhibitor molecules, and the nucleophilic centers of inhibitor molecules are normally electronegative groups, p-electrons in conjugated double bonds and heteroatoms with lone electron pairs, which are easily available to form covalent bonds [48]. Three active centres (negative region) within N and Br atoms of ABBT are observed than one within N atom of ABT, indicating ABBT molecule are readily transfer or sharing free electron pairs to copper to form

covalent bonds compared with ABT. It can be attributed to the conjugated effect with the existence of bromo-substitution.

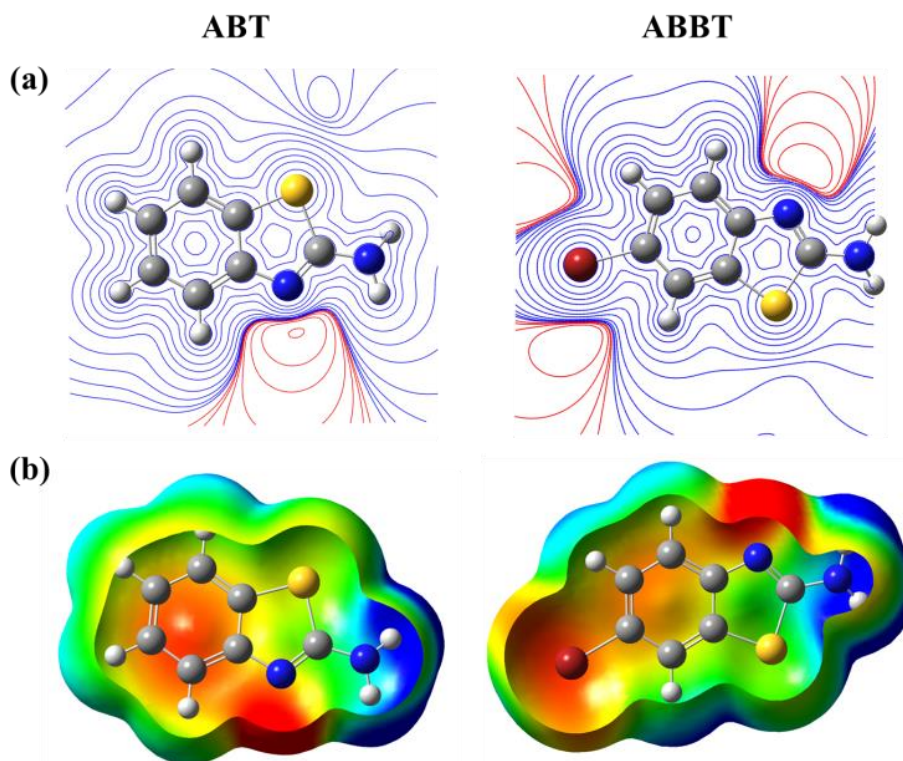


Figure 8. (a) Contour and (b) total electron density surface map of electrostatic potential for ABT and ABBT

Table 4. Quantum chemical parameters for the ABT and ABBT

	$E_{\text{HOMO}}(\text{eV})$	$E_{\text{LUMO}}(\text{eV})$	$\Delta E(\text{eV})$	$\mu(\text{Debye})$
ABT	-6.10	-0.78	5.32	1.94
ABBT	-6.15	-1.05	5.10	3.58

It is generally accepted that low E_{LUMO} demonstrates the ability of the molecule as an electron-accepter, whereas a tendency of the organic molecule to donate electrons to the suitable acceptor can be inferred by the high value of E_{HOMO} [45]. Therefore, the energy gap reflects the chemical stability of inhibitor molecule, and a lower value of ΔE shows that investigated inhibitor can be absorbed easily on metal surface [57]. The low values of energy gap in Table 4 obey the order: ABBT < ABT, indicating the high inhibition efficiencies of both inhibitors obtained by electrochemical techniques and weight loss measurements are extremely reasonable and the order of inhibition efficiency obtained above are theoretically confirmed.

Besides, the dipole moment is also an important index to investigate inhibition mechanism of metal corrosion. In present work, high values of μ in Table 4 lead to strong adsorption due to electronic

force [48]. The dipole moment for ABBT is higher than that for ABT, which is in accordance with inhibition ability of investigated inhibitors for copper in 3% NaCl solution.

3.7. Molecular dynamic simulation

In order to get further information about the interaction between these inhibitors and copper surface, molecular dynamic simulation were performed to model the adsorption mechanism of both ABT and ABBT on Cu (111) surface in 3% NaCl solution. The optimized equilibrium configuration of these inhibitors are shown in Fig. 9, it can be observed that ABBT molecule tends to be absorbed on the copper surface with a parallel mode, while there is a small contact angle between ABT molecule and copper substrate. As known, the parallel orientation of ABBT can maximize contact area between inhibitor molecule and copper to minimize copper surface area attacked by aggressive particles, so ABBT may be a more effective corrosion inhibitor than ABT. Moreover, the adsorption energy between Cu (111) surface and inhibitor molecule calculated from molecular dynamic simulation are -258.90 kJ/mol (ABT) and -286.57 kJ/mol (ABBT). The high absolute value of the adsorption energy of these inhibitors shows that strong adsorption of ABT and ABBT occurs on the metal surface [16, 39, 48, 58]. These results further confirm that more efficient inhibition ability can be obtained by ABBT compared with ABT for copper corrosion in 3% NaCl solution.

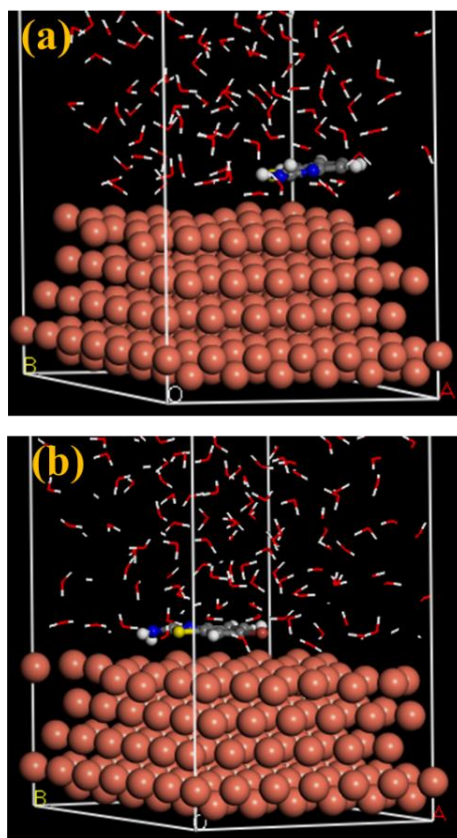


Figure 9. Equilibrium configuration for adsorption of (a) ABT and (b) ABBT on Cu (111) surface in 3% NaCl solution after optimization

4. CONCLUSIONS

The performance of ABT and ABBT as two corrosion inhibitors for copper in 3% NaCl solution was investigated by corrosion experiments and theoretical simulations. Both of these compounds are effective cathodic-type inhibitors and inhibition efficiencies obtained from weight loss, polarization curves and EIS measurements are in good agreement. The adsorption of these inhibitors on the copper surface in 3.0% NaCl solution obeys Langmuir adsorption isotherm. Besides, superior inhibitive performance of ABBT than ABT can be obtained. These results can further be explained as follows: 1) the values of ΔG_{ads}^0 demonstrate that chemisorption occurred between ABBT molecules and copper surface, while mixed adsorption mechanism (physisorption and chemisorption) were exhibited by ABT molecules. 2) Compared with ABT, ABBT can be easily and strongly adsorbed on copper surface inferred by some computed parameters, including ΔE , μ , and adsorption energy. 3) It can be seen from molecular dynamic simulations that the parallel adsorption orientation of ABBT can minimize copper surface area attacked by aggressive media, while there is a small contact angle between ABT molecule and copper substrate.

ACKNOWLEDGMENTS

This research was supported by Natural Science Foundation of China (No. 21376282) and the Research Fund for the Doctoral Program of Tongren University (No. trxyDH1510).

References

1. W. Chen, S. Hong, H. B. Li, H. Q. Luo, M. Li, N. B. Li, *Corrosion Science*, 61(2012) 53-62.
2. S. Herrmann, M. Kostrzewa, A. Wierschem, C. Streb, *Angewandte Chemie*, 53(2014) 13596-9.
3. M. A. Amin, *Journal of Applied Electrochemistry*, 36(2005) 215-26.
4. F. M. Bayoumi, A. M. Abdullah, B. Attia, *Materials and Corrosion*, 59(2008) 691-6.
5. W. Chen, S. Hong, H. Q. Luo, N. B. Li, *Journal of Materials Engineering and Performance*, 23(2013) 527-37.
6. S. L. Chi-Ucán, A. Castillo-Atoche, P. Castro Borges, J. A. Manzanilla-Cano, G. González-García, R. Patiño, et al., *Journal of Chemistry*, 2014(2014) 1-10.
7. A. Dafali, B. Hammouti, R. Mokhlisse, S. Kertit, *Corrosion Science*, 45(2003) 1619-30.
8. B. H., G. M., L. R., *Int J Electrochem Sci*, 8(2013) 7518 - 28.
9. B. Hammouti, A. Dafali, R. Touzani, M. Bouachrine, *Journal of Saudi Chemical Society*, 16(2012) 413-8.
10. O. A. Hazzazi, *Journal of Applied Electrochemistry*, 37(2007) 933-40.
11. K. F. Khaled, *Materials Chemistry and Physics*, 112(2008) 104-11.
12. K. F. Khaled, M. N. H. Hamed, K. M. Abdel-Azim, N. S. Abdelshafi, *Journal of Solid State Electrochemistry*, 15(2010) 663-73.
13. G. Kılınççeker, H. Demir, *Anti-Corrosion Methods and Materials*, 60(2013) 134-42.
14. C. Kun, S. Huyuan, Z. Xia, H. Baorong, *Int J Electrochem Sci*, 9(2014) 8106 - 19.
15. S. Hong, W. Chen, H. Q. Luo, N. B. Li, *Corrosion Science*, 57(2012) 270-8.
16. S. Hong, W. Chen, Y. Zhang, H. Q. Luo, M. Li, N. B. Li, *Corrosion Science*, 66(2013) 308-14.
17. C.-c. Li, X.-y. Guo, S. Shen, P. Song, T. Xu, Y. Wen, et al., *Corrosion Science*, 83(2014) 147-54.
18. E. M. Sherif, S.-M. Park, *Journal of The Electrochemical Society*, 152(2005) B428.

19. E. M. Sherif, S.-M. Park, *Corrosion Science*, 48(2006) 4065-79.
20. E.-S. M. Sherif, *Applied Surface Science*, 252(2006) 8615-23.
21. E.-S. M. Sherif, A. M. El Shamy, M. M. Ramla, A. O. H. El Nazhawy, *Materials Chemistry and Physics*, 102(2007) 231-9.
22. W. Li, L. Hu, S. Zhang, B. Hou, *Corrosion Science*, 53(2011) 735-45.
23. W. Qafsaoui, M. W. Kendig, H. Perrot, H. Takenouti, *Electrochimica Acta*, 87(2013) 348-60.
24. K. Rahmouni, M. Keddami, A. Srhiri, H. Takenouti, *Corrosion Science*, 47(2005) 3249-66.
25. G. Tansuğ, T. Tüken, E. S. Giray, G. Findıkkıran, G. Sığırcık, O. Demirkol, et al., *Corrosion Science*, 84(2014) 21-9.
26. H. Tian, W. Li, B. Hou, *Int J Electrochem Sci*, 8(2013) 8513 - 29.
27. Y. Qiang, S. Zhang, S. Xu, L. Yin, *RSC Advances*, 5(2015).
28. L. Hu, S. Zhang, W. Li, B. Hou, *Corrosion Science*, 52(2010) 2891-6.
29. F. Y. Cui, L. Guo, S. T. Zhang, *Materials and Corrosion*, 65(2014) 1194-201.
30. A. Döner, R. Solmaz, M. Özcan, G. Kardaş, *Corrosion Science*, 53(2011) 2902-13.
31. A. Ongun Yüce, B. Doğru Mert, G. Kardaş, B. Yazıcı, *Corrosion Science*, 83(2014) 310-6.
32. M. Yadav, D. Sharma, S. Kumar, *Korean Journal of Chemical Engineering*, 32(2015) 993-1000.
33. Jelena Nakomčić, Gyöngyi Vastag, Abdul Shaban, L. Nyikos, *International Journal of Electrochemical Science*, 10(2015) 17.
34. M. Finšgar, D. Kek Merl, *Corrosion Science*, 83(2014) 164-75.
35. E. Abdullayev, V. Abbasov, A. Tursunbayeva, V. Portnov, H. Ibrahimov, G. Mukhtarova, et al., *ACS applied materials & interfaces*, 5(2013) 4464-71.
36. H. Tian, W. Li, K. Cao, B. Hou, *Corrosion Science*, 73(2013) 281-91.
37. X. Zheng, S. Zhang, W. Li, M. Gong, L. Yin, *Corrosion Science*, 95(2015) 168-79.
38. X. Zheng, S. Zhang, W. Li, L. Yin, J. He, J. Wu, *Corrosion Science*, 80(2014) 383-92.
39. D. Wang, B. Xiang, Y. Liang, S. Song, C. Liu, *Corrosion Science*, 85(2014) 77-86.
40. P. Song, X.-Y. Guo, Y.-C. Pan, S. Shen, Y. Sun, Y. Wen, et al., *Electrochimica Acta*, 89(2013) 503-9.
41. S. Liu, H. Sun, L. Sun, H. Fan, *Corrosion Science*, 65(2012) 520-7.
42. S. Zhang, Z. Tao, W. Li, B. Hou, *Applied Surface Science*, 255(2009) 6757-63.
43. S. Zhang, Z. Tao, S. Liao, F. Wu, *Corrosion Science*, 52(2010) 3126-32.
44. E. M. Sherif, S.-M. Park, *Journal of The Electrochemical Society*, 152(2005) B205.
45. L. Guo, S. Zhu, S. Zhang, *Journal of Industrial and Engineering Chemistry*, 24(2015) 174-80.
46. C. He, Z. Tian, B. Zhang, Y. Lin, X. Chen, M. Wang, et al., *Industrial & Engineering Chemistry Research*, 54(2015) 1971-81.
47. P. B. Matad, P. B. Mokshanatha, N. Hebbar, V. T. Venkatesha, H. C. Tandon, *Industrial & Engineering Chemistry Research*, 53(2014) 8436-44.
48. D. Daoud, T. Douadi, H. Hamani, S. Chafaa, M. Al-Noaimi, *Corrosion Science*, 94(2015) 21-37.
49. S. Hari Kumar, S. Karthikeyan, *Industrial & Engineering Chemistry Research*, 52(2013) 7457-69.
50. P. M. Krishnegowda, V. T. Venkatesha, P. K. M. Krishnegowda, S. B. Shivayogiraju, *Industrial & Engineering Chemistry Research*, 52(2013) 722-8.
51. S. Shen, X.-y. Guo, P. Song, Y.-C. Pan, H.-q. Wang, Y. Wen, et al., *Applied Surface Science*, 276(2013) 167-73.
52. M. Bozorg, T. Shahrabi Farahani, J. Neshati, Z. Chaghazardi, G. Mohammadi Ziarani, *Industrial & Engineering Chemistry Research*, 53(2014) 4295-303.
53. R. Chami, F. Bensajjay, S. Alehyen, M. El Achouri, A. Bellaouchou, A. Guenbour, *Colloids and Surfaces A: Physicochemical and Engineering Aspects*, 480(2015) 468-76.
54. X. Zheng, S. Zhang, M. Gong, W. Li, *Industrial & Engineering Chemistry Research*, 53(2014) 16349-58.
55. T. Zhihua, z. Shengtao, L. Weihua, *Corrosion Science*, 51(2009) 8.

56. X. Ren, S. Xu, S. Chen, *Rsc Advances*, 5(2015).
57. L. Guo, S. Zhu, S. Zhang, Q. He, W. Li, *Corrosion Science*, 87(2014) 366-75.
58. D. Q. Zhang, H. j. Zeng, L. Zhang, P. Liu, L. X. Gao, *Colloids and Surfaces A: Physicochemical and Engineering Aspects*, 445(2014) 105-10.

© 2016 The Authors. Published by ESG (www.electrochemsci.org). This article is an open access article distributed under the terms and conditions of the Creative Commons Attribution license (<http://creativecommons.org/licenses/by/4.0/>).